

# Optical induction of 3D rotational symmetry refractive lattices by combined interferometric-mask method in doped $\text{LiNbO}_3$ crystals

A. Badalyan · R. Hovsepyan · P. Mantashyan ·  
V. Mekhitarian · R. Drampyan

Received: 19 July 2013 / Accepted: 12 September 2013 / Published online: 8 October 2013  
© Springer-Verlag Berlin Heidelberg 2013

**Abstract** A novel combined interferometric–mask method for the formation of micro- and nanometric scale three-dimensional (3D) rotational symmetry quasi-crystal-line refractive lattice structures in photorefractive materials is demonstrated experimentally. The method is based on micrometric scale spatial modulation of the light by amplitude mask in the radial directions and along the azimuthal angle and the use of counter-propagating beam geometry building up Gaussian standing wave, which defines the light modulation in the axial direction with half-wavelength periodicity. 3D intensity pattern can be represented as numerous mask-generated 2D quasi-periodic structures located in each anti-node of the standing wave. The formed 3D intensity distributions of the optical beams can be imparted into the photorefractive medium thus creating the micro- and sub-micrometric scale 3D refractive index volume lattices. The used optical scheme allows also the formation of 2D lattices by removing the back-reflecting mirror. 2D and 3D refractive lattices were recorded with the use of 532 nm laser beam and rotational symmetry mask in doped lithium niobate crystals and were tested by the probe beam far-field diffraction pattern imaging and direct observation by phase microscope. The formed rotational symmetry 3D refractive structures have the periods of 20–60  $\mu\text{m}$  in the radial directions, 60  $\mu\text{m}$  along the azimuthal angle and half-wavelength 266 nm in the axial direction.

## 1 Introduction

Materials with artificial refractive index modulation—photonic crystals [1–4] and optically induced refractive lattices [5–10]—have become the subject of extensive research in the last two decades. Two- and three-dimensional (2D, 3D) photonic crystals and refractive lattice structures offer new possibilities to route, control and steer light and are of great interest for many applications, including guiding and trapping systems, photonic bandgap materials, all-optical devices, information storage and processing, telecommunication systems, optical computers, etc. [1–10]. While different fabrication methods, such as etching processes, electronic beam and UV lithography in high refractive index materials [2–4] have been utilized to produce photonic crystals with permanently fixed periodic structures, some future applications certainly require an increased flexibility and the possibility to tune and adapt the photonic lattices in real time.

From these reasons, the approach of an optical induction of refractive lattices in photosensitive materials (holographic technique) becomes particularly attractive [5–10]. The illumination of photorefractive medium by spatially modulated light beam leads to the corresponding refractive index modulation thus creating refractive lattices. Some of most promising photosensitive materials are photorefractive crystals [5–10], liquid crystals [11, 12] and composite polymer materials, including polymer-dispersed [13] and polymer-stabilized liquid crystals [14–16], photopolymerizable zol-gel glass [17] and its modifications [18–20], as well as atomic vapors [21, 22]. In spite of these methods provide relatively low refractive index contrast, compared with the techniques of lithography or etching in high refractive index materials, nevertheless, such refractive lattices are very promising for high capacity information

---

A. Badalyan · R. Hovsepyan · P. Mantashyan ·  
V. Mekhitarian · R. Drampyan (✉)  
Institute for Physical Research, National Academy of Sciences  
of Armenia, 0203 Ashtarak-2, Armenia  
e-mail: rafael\_drampyan@yahoo.com

storage and readout [23], for controlling and manipulating the flow of light [2, 3, 6, 7], for formation of two-dimensional spatial solitons (see [24–28] and references therein), etc.

The computer-generated holographic technique [7, 29] and lately suggested Bessel standing wave method [30] are very successful for creation of 2D spatial periodic structures in photorefractive materials. The non-diffracting Airy [31], Weber and Mathieu [32] beams were also suggested for formation of 1D- and 2D-specific refractive lattice structures.

Recently, there has been considerable interest to the rotational symmetry photonic structures, which consists of non-periodic structures analogous to the quasi-crystals [33]. The higher rotational symmetry photonic quasi-crystalline structures lead to isotropic and complete photonic bandgaps even in the materials with low refractive index contrast [34–36].

The fabrication of 3D periodic and quasi-periodic structures, especially of higher rotational symmetry, remains a real challenge as many of the conventional methods become either technically unsuitable or extremely complicated. The technique of multi-exposure of two-beam [37] and multi-beam interference patterns [38] was realized for fabrication of 2D and 3D quasi-periodic structures in photosensitive materials. 3D optically induced reconfigurable nonlinear photonic lattices [39], as well as quasi-crystalline photonic structures [40] based on computer-generated phase only spatial light modulator (SLM), were formed in cerium-doped strontium barium niobate photorefractive crystal.

Recently, we suggested the combined interferometric-mask method [41] based on spatial light modulation by amplitude mask in the transverse plane and the use of counter-propagating beam geometry building up Gaussian standing wave, which defines the light intensity modulation in the axial direction with half-wavelength periodicity. Thus, the created 3D intensity pattern can be represented as numerous mask-generated 2D periodic or quasi-periodic structures located in each anti-node of the standing wave. The formed intensity patterns can be imparted into the photosensitive medium thus creating micro- and nanoscale 3D refractive index volume lattices. The main idea, the sketch of experimental technique and first results on recording of 3D refractive lattices with the use of sevenfold rotational symmetry mask in photorefractive Fe-doped lithium niobate crystals were presented in [41].

In this paper, we present the detailed experimental studies of 3D refractive lattices formation in doped lithium niobate (LN) crystals with the use of twofold rotational symmetry amplitude mask and 532 nm cw laser beam for recording. This mask while having strong periodicity along the azimuthal angle is an example of multi-periodical structures along the radial directions. The formed 3D

rotational symmetry refractive structures have 20–60  $\mu\text{m}$  periods in the radial directions, 60  $\mu\text{m}$  period along the azimuthal angle and half-wavelength 266 nm period in the axial direction. The recorded 3D refractive lattices were tested by the probe beam far-field diffraction pattern imaging and direct observation by phase microscope.

## 2 Main approach

Unlike the conventional techniques based on multi-exposure of two-beam [37] and multi-beam interference patterns [38], as well as on computer-generated reconfigurable phase engineering patterns [39, 40], which require a complicated optical setups, a new combined interferometric-mask (CIM) method for creation of 3D periodic and quasi-periodic structures in photorefractive materials is suggested and realized. The method is based on illumination of the photorefractive crystal through the mask having micrometric scale speckles disposition with different rotational symmetries (RS) by Gaussian beam in combination with back-reflecting mirror. The mask provides the micrometric scale spatial modulation of the light in the radial directions and along the azimuthal angle. The counter-propagating beam geometry builds up Gaussian standing wave, which defines the light intensity modulation in the axial direction with sub-micrometric scale half-wavelength periodicity. The experimental scheme is given in Fig. 1a. Schematic of 2D transverse intensity distribution is shown in Fig. 1b. The created 3D intensity pattern is a set of numerous mask-generated 2D quasi-periodic structures located in each anti-node of the standing wave (Fig. 1c).

The formed intensity patterns can be imparted into the photorefractive medium thus creating the micro- and sub-micro scale 2D and 3D refractive index volume lattices.

Photorefractive crystals are widely investigated for applications in the holographic recording [5–9] due to the possibility of multiple recording and erasure of the holograms. Illumination of these materials by inhomogeneous light redistributes photo-charges excited by photo-ionization. The migration of photo-charges mainly by photovoltaic effect along *C*-axis of the crystal builds up internal electric fields and so changes the refractive index via electro-optic effect, thus providing the induction of refractive lattice structures [5–8].

Doped lithium niobate crystals have been extensively studied as materials for volume holographic memory applications because of their excellent photorefractive properties [6–8]. Fe is the most effective in producing large improvements in both the sensitivity and the maximum diffraction efficiency of optical recording. Last decades, the development of 532 nm cw intense laser sources and relatively high absorption properties of Fe doped lithium

**Fig. 1 a** Experimental setup for the optical induction of 3D lattices by CIM method. The inset shows the experimentally obtained Gaussian intensity distribution of 532 nm laser beam obtained by beam profiler Thorlabs BP109-VIS.

**b** Schematic of the fragment of 2D light arrays formed inside the crystal by twofold RS mask. **c** Schematic of two neighboring anti-nodes of standing wave, where the mask-created quasi-periodic structures are located. The recorded 3D refractive lattice is modulated in the radial direction  $R$ , along the azimuthal angle  $\varphi$  and in the axial  $Z$  directions. The scale along the direction of standing wave ( $Z$ -axis) is enlarged relative to  $R$  and  $\varphi$  directions

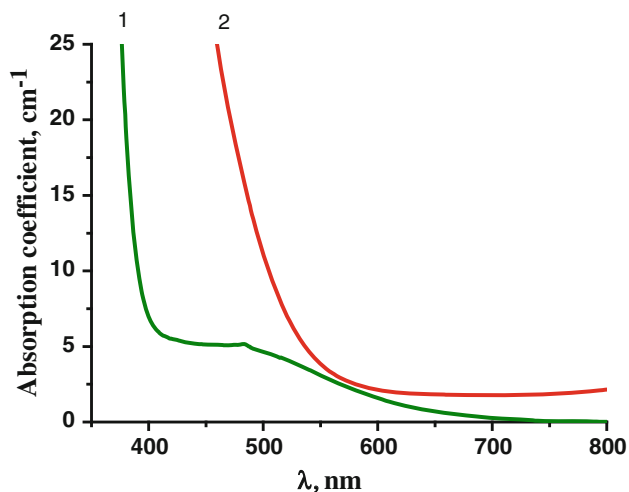
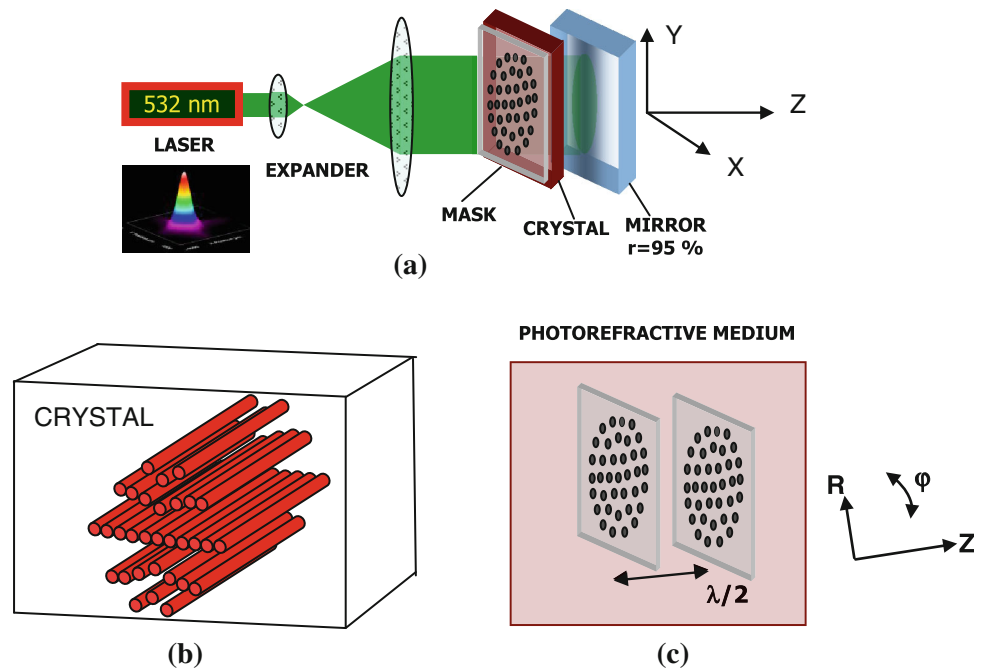


**Fig. 2** Absorption spectra of LN crystals singly doped by 0.05 wt% Fe (curve 1) and doubly doped by 0.05 wt% of Fe and Cu (curve 2) used in our experiment. The spectra were measured by spectrometer Specord M40 with spectral range of 190–900 nm

niobate (LN:Fe) crystal in the green optical range makes these crystals very convenient for formation of refractive lattices.

From these reasons, the creation of 3D lattices by CIM method was performed in  $Y$ -cut LN:Fe crystals with use of cw green 532 nm laser beam. Some measurements were performed also in doubly doped by Fe and Cu lithium niobate (LN:Fe:Cu) crystal.

The single-domain lithium niobate crystals doped with 0.05 wt% of  $\text{Fe}_2\text{O}_3$  (LN:Fe) and 0.05 wt% of  $\text{Fe}_2\text{O}_3$  and CuO (LN:Fe:Cu) used in the experiments have been grown by

Czochralski method and annealed in the oxygen atmosphere at 1,000 °C during 45 min. The single crystal boule was oriented by X-ray diffraction, and then, samples were cut and polished according to specific requirements of the investigations.  $Y$ -cut crystals oriented along the crystal surface were used in our experiments. Figure 2 shows the absorption spectra of LN crystals singly doped with 0.05 wt% of Fe and doubly doped with 0.05 wt% of Fe and Cu.

### 3 Preparation and optical testing of 2D rotational symmetry masks

From one-to-tenfold axial symmetry masks were generated by computer graphic technique. The masks consisted of transparent holes, which were periodically disposed along the hypothetical equidistantly positioned concentric circles surrounding the central hole. The number of holes on the  $i$ th circle was equaled  $M_i = iJ$ , where  $i = 1, 2, 3, \dots$  is integer and  $J$  is the symmetry order of the mask. The masks of reduced size (0.6 cm in diameter) with  $i = 100$  were printed by high resolution printer (3,300 dpi) on the transparent film. Both the positive and negative masks were prepared. The prepared reduced size negative masks had a distance of 20–60  $\mu\text{m}$  between 10  $\mu\text{m}$  transparent holes on the opaque disk. Figure 3a–d shows the fragments of 2, 3, 6 and sevenfold RS masks. Higher is the rotational symmetry of the mask larger is the total number of the holes. For example, the whole twofold RS mask consists of  $\sim 10,000$  holes disposed along the 100 hypothetical concentric circles with 60  $\mu\text{m}$  periodicity.

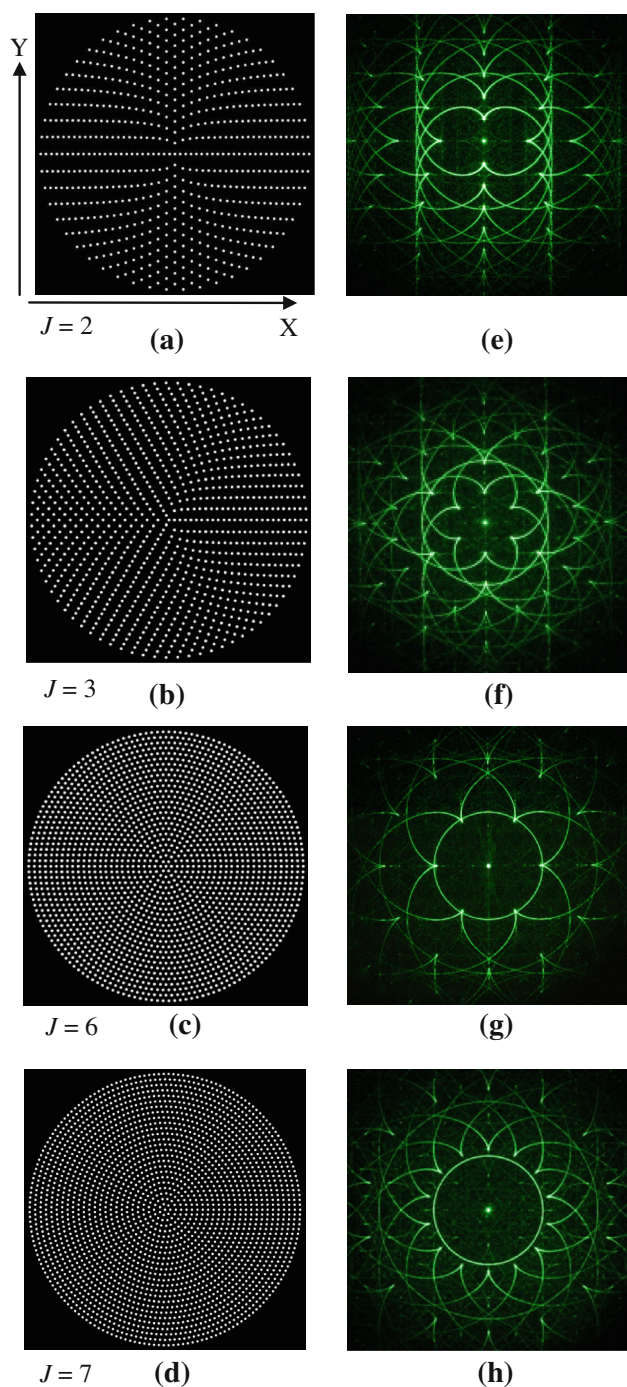


**Fig. 3** a–d Fragments of enlarged patterns of computer-generated negative masks with  $J = 2, 3, 6$  and sevenfold rotational symmetries. The masks had a diameter of 0.6 cm and a distance around 20–60  $\mu\text{m}$  between  $\sim 10 \mu\text{m}$  transparent holes. e–h Corresponding diffraction patterns from the masks obtained by *green* Gaussian laser beam in the far field

The masks were tested by observing the diffraction patterns from the masks in the far field by 532 nm green cw laser beam. Diffraction patterns from two, three, six and sevenfold RS masks (Fig. 3a–d) obtained by green

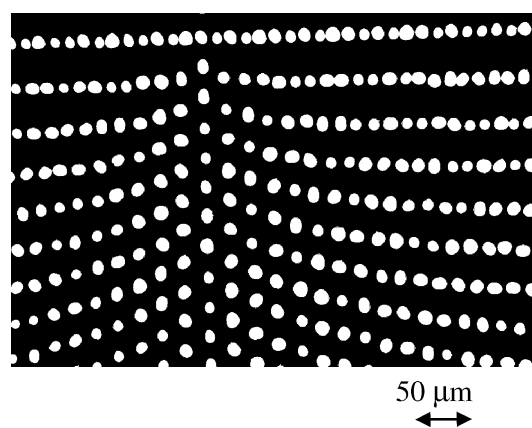


**Fig. 4** Fragment of microscope image of the twofold RS negative mask printed on the film

Gaussian laser beam in the far field are shown in Fig. 3(e–h), respectively.

The obtained high-contrast diffraction patterns (Fig. 3e–h) confirm the high quality of the prepared masks. Figure 4 shows the microscope image of the fragment of twofold RS negative mask printed on the transparent thin film.

#### 4 Optical induction of 2D and 3D refractive lattices

Twofold RS mask was used for creation of 3D lattices in Y-cut LN:Fe crystal by combined interferometric–mask technique. This mask while having strong periodicity along azimuthal angle is an example of multi-periodical structures along the transverse  $X$  and  $Y$  directions. Experimental setup for optical recording of 3D lattices is shown in Fig. 1a. For comparison, the recording of 2D lattices using only the mask technique, without formation of standing wave, was also performed by removing the back-reflecting mirror (see Fig. 1a, b). Cw single-mode 100 mW green 532 nm laser (Spectralus SP 532 BFL) was used for realization of the experiments. The beam power transmitted through the mask was measured of 1.26 mW. The lattices were recorded in Y-cut 0.05 wt% LN:Fe crystal with the size of  $14 \times 10 \times 0.5 \text{ mm}^3$ . There were two reasons for the use of the crystal with thickness of 0.5 mm. The first reason was to avoid the interference effects of the beams, diffracted from the holes of the mask, inside the crystal (noise holograms). The Rayleigh range for  $w \sim 10 \mu\text{m}$  circular holes of mask estimated by  $kw^2/2$ , where  $k = 2\pi/\lambda$  is equaled to 0.6 mm for  $\lambda = 532 \text{ nm}$ . The second reason was to eliminate the mask self-replicated images inside the crystal due to Talbot effect [42, 43]. Both mentioned extra structures can lead to the additional scattering noise in the crystal with larger thickness. Recording was performed also in

2-mm-thick LN:Fe:Cu crystal doped with 0.05 wt% of Fe and Cu, and the dispersive properties of refractive lattice were studied by white light from light emitted diode.

The profile of single-mode green 532 nm Gaussian beam is shown in the inset of Fig. 1a. The laser beam was expanded by confocal lenses and after passing through the mask illuminated the crystal. The mask and back-reflecting mirror with  $r = 95\%$  reflection coefficient were practically in touch with the crystal. The mask was oriented in the  $X$ – $Y$  plane as shown in Fig. 3a. Optical  $C$ -axis of the crystal was oriented along the crystal surfaces. The orientations of optical  $C$ -axis along both  $X$  and  $Y$  directions were used during recording. Polarization of the recording laser beam was directed along  $X$  direction. The duration of recording was 30–60 min, which provides the saturated regime of recording.

## 5 Optical testing of recorded lattices

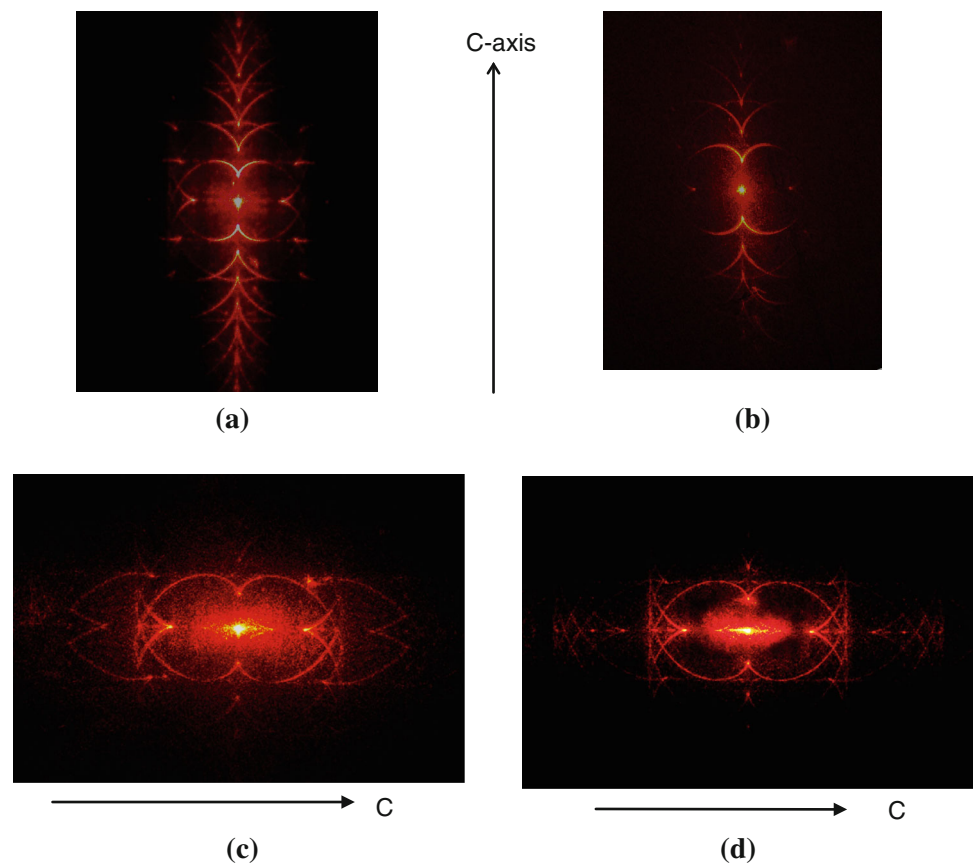
The recorded refractive lattices were tested with the use of Thorlabs HRP-170 single-mode He–Ne 633 nm laser beam by observing the forward diffracted pattern from the 2D and 3D lattices in the far field. Readout was performed using both ordinary and extraordinary polarized beams.

The red 633 nm laser beam was used to minimize the erasure of the recorded lattices during readout.

Figure 5a, b shows the examples of the diffraction patterns obtained by 16.5 mW red laser beam from 2D refractive lattices recorded by the mask technique (a) and from 3D lattices recorded by CIM method (b) with the use of twofold RS mask and 0.5-mm-thick LN:Fe crystal.  $C$ -axis of the crystal was directed along  $Y$  direction during recording. The polarization of the readout 633 nm beam was in the plane (e-polarization) defined by  $C$ -axis of the crystal and wave vector of the beam. The diffraction patterns from 2D lattices (Fig. 5a) showed more diffraction orders in the direction of optical  $C$ -axis of the crystal compared with diffraction from 3D lattices (Fig. 5b).

The results of optical testing of 2D and 3D recorded lattices when the  $C$ -axis of the crystal was directed along  $X$  direction of twofold RS mask during recording are shown in Fig. 5c, d. Readout was performed by extraordinary testing beam. For 2D lattice, the diffraction orders are directed along horizontally oriented  $C$ -axis of the crystal and are limited by second-order diffraction. 3D lattice shows only the first-order diffraction. The background scattered noise in diffraction patterns is essentially less for 3D lattices compared with 2D lattice.

**Fig. 5** Diffraction patterns from 2D (a, c) and 3D (b, d) refractive lattices recorded by mask and CIM techniques, respectively, in 0.5-mm-thick LN:Fe crystal for different orientations of  $C$ -axis of the crystal during recording—along  $Y$  direction (a, b) and  $X$  direction (c, d) of twofold RS mask. Readout was performed by extraordinary testing beam (e-polarization). Arrows show the direction of optical  $C$ -axis of the crystal relative to the diffraction patterns. The scales in the figures are different



The experimental measurements showed that the polarization of diffracted beams coincides with the polarization of the testing beam.

The obtained diffraction patterns from the recorded lattices can be compared with diffraction pattern obtained by green laser beam from original twofold RS negative mask and are shown in Fig. 3e.

## 6 Measurements of diffraction efficiency and erasure of recorded lattices

The diffraction efficiency measurements of recorded 2D and 3D lattices, as well as the time evolution of 2D lattices formation, were performed with the use of different schemes.

1. The first measurements were performed by measuring the forward diffracted power from the recorded lattices with the use of 633 nm Gaussian e-polarized testing beam with input power  $P_{\text{input}} = 16.5$  mW. The diffracted power  $P_{\text{dif}}$  was measured as total forward scattered power  $P_s$  minus the background power transmitted through the “clean” part of crystal without recorded lattice  $P_{\text{bg}}$ . The diffraction efficiency calculated as  $\eta = \{P_{\text{dif}}/P_{\text{input}}\} \times 100\%$  is equaled to 2.3 and 1.15 % for 2D and 3D lattices, respectively.
2. The study of the time evolution of 2D lattice formation during recording by 532 nm beam in 0.5-mm-thick LN:Fe crystal was also performed. Scheme of the measurement is shown in Fig. 6a. The total power  $P_{\text{total}}$  of 532 nm recording beam transmitted through the mask and crystal during recording process was measured (see Fig. 6a). This power consists of both the constant power  $P_{\text{dif-mask}}$  diffracted from the mask (see Fig. 3e) and variable power  $P_{\text{dif-latt}}$  diffracted from the refractive lattice during recording in the crystal. The measured difference  $P_{\text{dif}} = (P_{\text{total}} - P_{\text{dif-mask}})$  characterizes the diffracted power. The time evolution of diffracted power is shown in Fig. 6b and demonstrates the increase in diffracted power during 400 s and its further saturation.

The erasure of the recorded lattices during illumination by 1.2 mW uniform green and red beams has also been measured and is shown in the Fig. 6c. The erasure curves are approximated by exponential function  $P_{\text{dif}} = A \exp(-t/\tau_e)$  with  $A = 0.031$  mW and erasure constant of  $\tau_e = 1,200$  s for green beam (curve 1), and  $A = 0.031$  mW and erasure constant of  $\tau_e = 20,000$  s for red beam (curve 2), respectively.

## 7 Dispersive properties of the volume refractive lattice

The dispersive properties of the recorded volume refractive lattices have been studied by diffraction testing with the use

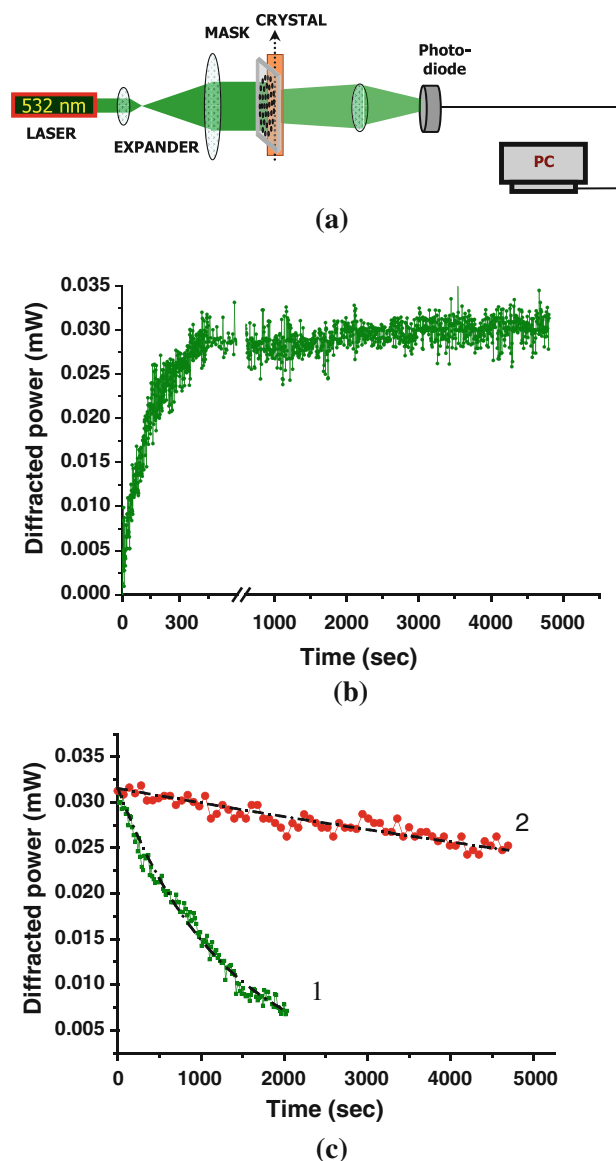


**Fig. 6** **a** Experimental scheme for simultaneous recording of 2D lattice by 532 nm beam in LN:Fe crystal and study of time evolution of diffracted power by measuring the 532 nm beam power transmitted through the mask and crystal during recording. The measurements were performed by power meter PM 120 D (Thorlabs) connected to PC. **b** Time evolution of diffracted power during recording. **c** Erasure of the recorded lattices by 1.2 mW green (curve 1) and red (curve 2) Gaussian laser beams. The approximating exponential curves are shown by dotted-dashed lines

of white light from light emitted diode that was formed by mixing of three color (red, green and blue) lights (RGB LED) with 1 W light power and FWHM spectral bandwidth approximately equaled to 24–27 nm for all three colors peaked at 640, 570 and 480 nm. The lattices were recorded with the use of twofold RS mask in doubly doped LN:Fe:Cu crystal by 532 nm laser beam. The light emitted from the LED source after passing through the 1 mm diaphragm

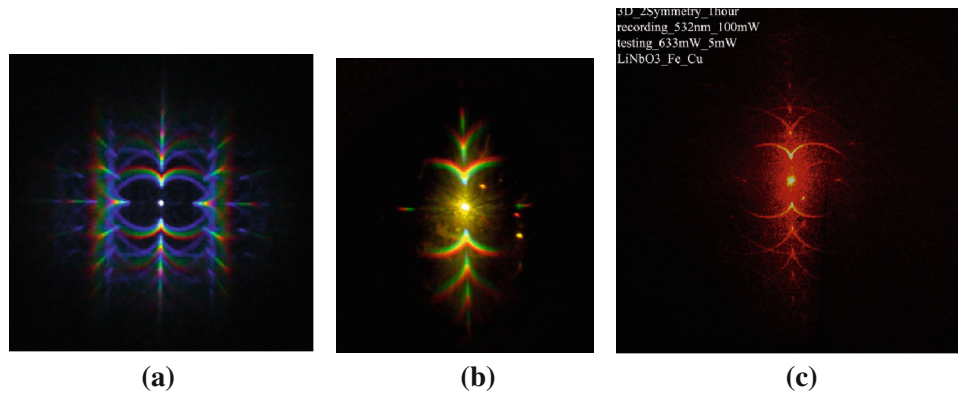


**Fig. 7** **a** Far-field diffraction pattern from twofold RS mask obtained by RGB LED source. **b** Diffraction pattern obtained by RGB LED source from 3D refractive lattice recorded into the LN:Fe:Cu crystal by twofold symmetry mask and *green* laser beam. The absence of

*blue color* contour is due to strong absorption of *blue light* in the crystal. **c** Diffraction pattern obtained by 5 mW probe *red* laser beam from 3D photonic lattice

illuminates the mask placed 150 cm far from the diaphragm. Figure 7a shows the far-field diffraction pattern obtained from twofold RS negative mask by white light from RGB LED source. Figure 7b shows the far-field diffraction pattern obtained with the use of RGB LED source from 3D lattice recorded in LN:Fe:Cu crystal. The diffraction pattern reveals the dispersive properties of recorded lattice and shows approximately equal diffraction efficiency for visible spectral range. The absence of blue color contour is due to strong absorption of blue light in the crystal (Fig. 2). For comparison, the diffraction pattern obtained by 5 mW red 633 nm probe beam is shown in Fig. 7c.

## 8 Observation of the recorded refractive lattices by phase microscope

Direct observation of 2D and 3D lattices recorded in LN:Fe 0.5-mm-thick crystal by multi-system phase microscope (Versamet Union 2) was also performed. The interference contrast observation was performed. The microscope allowed strictly reveals the refractive index lattice with estimated refractive index modulation of  $\Delta n \sim 10^{-4} - 10^{-5}$  (see Sect. 9.2), however, did not allow to perform the quantitative measurements. However, phase microscope allows the measurements of periodicity of the observed structure with accuracy of 1  $\mu\text{m}$ . The results for twofold symmetry 2D and 3D photonic lattices are shown in Fig. 8a, b. Phase microscope image of 3D lattice (b) shows higher contrast compared with the 2D lattice image (a).

More precise measurements of refractive index change are planned to perform in our further studies. Such information can be obtained by quantitative phase imaging, for example, with digital holographic microscopy [44] or quadriwave lateral shearing interferometry [45].

## 9 Discussion

### 9.1 Physical mechanism of the refractive lattices formation in the doped LN crystal

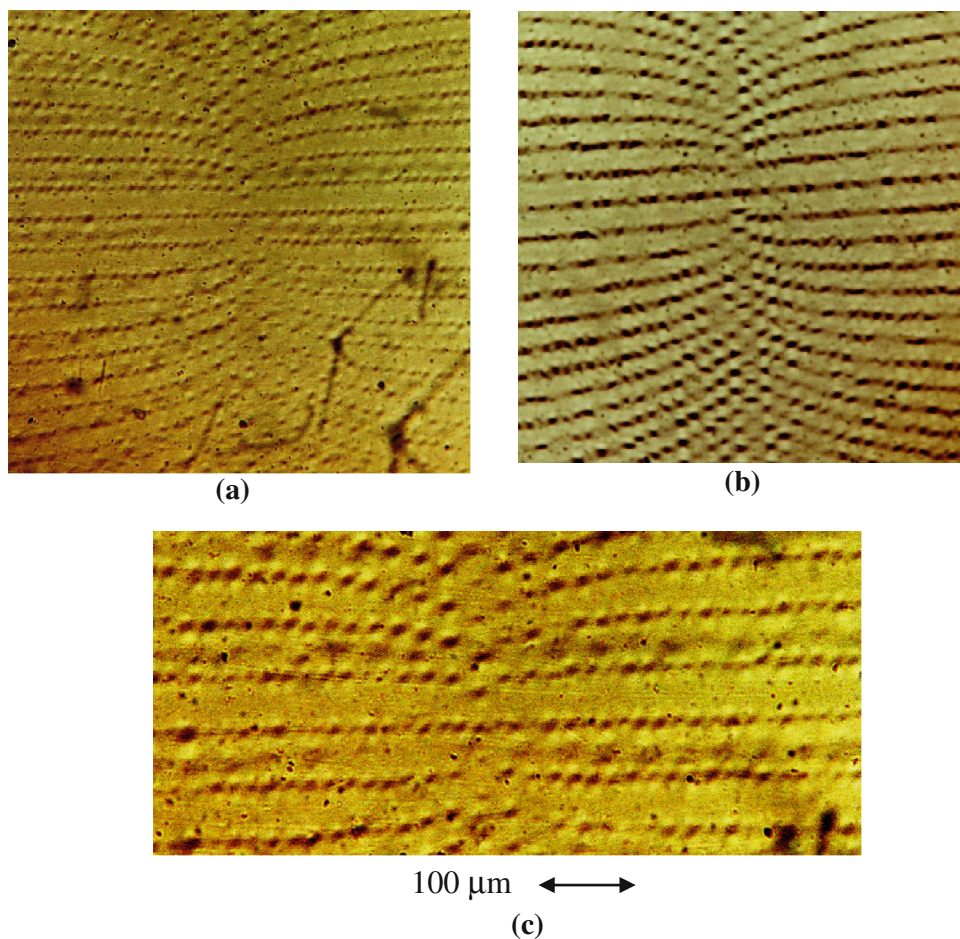
The physical mechanism of the refractive lattices formation in the photorefractive materials under illumination by intensity-modulated light is based on the electro-optic effect. Fe ions occur in LN crystal in different valence states of  $\text{Fe}^{2+}$  and  $\text{Fe}^{3+}$ . In illuminated regions of the crystal, the green light excites the electrons from  $\text{Fe}^{2+}$  to conduction band. Electrons migrate in the conduction band and finally are trapped by  $\text{Fe}^{3+}$  in non-illuminated dark zones in the crystal.

The redistribution of the charges builds up an internal space charge electric field  $E_{sc}$ , which changes the refractive index via electro-optic effect for both  $o$  and  $e$  polarizations  $\Delta n_o = 0.5n_o^3r_{13}E_{sc}$  and  $\Delta n_e = 0.5n_e^3r_{33}E_{sc}$ , where  $r_{13}$  and  $r_{33}$  are electro-optic coefficients,  $n_o = 2.32$  and  $n_e = 2.22$  [46]. In the Fe-doped LN crystal, the change in extraordinary index is larger than the change in ordinary index by a factor of four [47, 48], and the induced refractive index change  $\Delta n$  is mainly due to the distortion of extraordinary index of refraction.

The electric field is induced due to spatial charge separation caused by photovoltaic effect and diffusion of the charge carriers [48, 49]. The diffusion effect for the charge carriers can be neglected for grating spatial frequencies  $K = 1/d$  having the values less than  $\sim 10^5$  lines/cm, where  $d$  is the grating period [48].

During recording of 2D refractive lattices with the use of twofold RS mask with the periods of 20–60  $\mu\text{m}$  in the transverse plane, the photovoltaic effect which takes place along the  $C$ -axis of the crystal is the main process for charge transport, since the spatial frequency  $K \sim 10^3$  lines/cm.

**Fig. 8** Fragments of phase microscope images of  $X$ – $Y$  plane of 2D (a) and 3D (b) photonic lattices recorded inside of 0.5-mm-thick LN:Fe crystal by twofold RS mask and green laser beam. c Enlarged pattern of the central part of the image shown in (a). Obtained images of refractive lattices should be compared with microscope image of twofold symmetry mask shown in Fig. 4



During recording of 3D lattices, the half-wavelength period in the axial direction provides enough high spatial frequency of  $\sim 4 \times 10^4$  lines/cm, and in addition to the photovoltaic effect along the crystalline  $C$ -direction, the diffusion effect also gives contribution to the grating formation in the axial direction, however, with less efficiency. The contribution of these two mechanisms in refractive lattices formation was studied in detail for 1D and 2D lattices formation by Bessel beam technique in [30, 50].

The nonuniform light distribution formed by the used mask has a speckle pattern. The spatial distribution of the trapped electrons and the positive ionized centers leads to the corresponding refractive index change for each speckle.

As it is shown in [47], where the refractive index changes induced by 633 nm laser beam with 0.2 mm diameter in lithium niobate and lithium tantalate crystals are studied, the refractive index change  $\Delta(n_e - n_0)$  is negative, has maximum value in the center of light spot and decreases nearly symmetrically toward the spot edges. However, the gradient of  $\Delta(n_e - n_0)$  is different along and perpendicular to the  $C$ -axis of the crystal.

Along  $C$ -axis,  $\Delta(n_e - n_0)$  decreases to zero sharply at the light spot edges forming rectangular distribution with half-width equaled to the beam size. The overall distribution has also 3–4 times smaller positive wings. In the direction perpendicular, the  $C$ -axis  $\Delta(n_e - n_0)$  decreases to zero slowly with the refractive index change bell-shaped distribution, in which half-width is approximately two times larger than the beam size. The value of  $\Delta(n_e - n_0)$  remains negative. Similar results are obtained for LN:Fe crystal in [51].

The results obtained in [47, 51] allow to suppose that the refractive lattice formed by the used twofold RS mask can be considered as the rectangular grating along  $C$ -axis and as a sinusoidal grating in the direction perpendicular to  $C$ -axis of the crystal.

## 9.2 Diffraction efficiency

The refractive index change  $\Delta n$  is determined by  $\Delta n = k_2 \alpha W$ , where  $k_2$  is photorefractive sensitivity,  $W$  is energy density and  $\alpha$  is absorption coefficient [48]. The coefficient  $k_2$  is found to be independent of the impurity concentration and



dependent only on the nature of absorbing centers and, for Fe-doped LN crystal, is measured of  $k_2 = 1.4 \times 10^{-5} \text{ cm}^3/\text{J}$  for 514 nm in [48]. Absorption coefficient  $\alpha$  is measured of  $3.74 \text{ cm}^{-1}$  at 532 nm for the sample with 0.05 wt% of Fe in LN crystal used in the present experiment (see Fig. 2). The green laser power transmitted through the mask is measured of 1.26 mW. The energy invested into the crystal during 400 s illumination, when the saturation is achieved (Fig. 6b), is calculated as  $0.5 \text{ J/cm}^2$ . The energy density estimated of  $1.4 \text{ J/cm}^2$  for illuminated area on the crystal of  $0.36 \text{ cm}^2$ . Thus, the value of  $\Delta n$  can be estimated  $\sim 0.7 \times 10^{-4}$ . In fact, this value for 532 nm wavelength should be somewhat less since  $k_2$  decreases with the increase in wavelength [48] similar to the absorption coefficient behavior.

The value of  $\Delta n$  was calculated from the measured diffraction efficiency  $\eta = 2.3 \times 10^{-2}$  using Kogelnik's formulae  $\eta = \sin^2(\pi L \delta n/\lambda \cos \theta)$  for 2D transmission lattice and  $\eta = \tanh^2(\pi L \delta n/\lambda \cos \theta)$  for 3D reflection lattice [10, 52], where  $L$  is sample thickness and  $\theta$  is the angle of incidence to the grating. Estimation gives  $\Delta n = 0.6 \times 10^{-4}$  and  $\Delta n = 0.3 \times 10^{-4}$  for 2D and 3D lattices, respectively, for  $L = 0.5 \text{ mm}$ ,  $\theta = 0^\circ$ . For 2D lattice, the obtained value of  $\Delta n$  corresponds to the refractive sensitivity  $S = \Delta n/W = 0.4 \times 10^{-4} \text{ cm}^2/\text{J}$  estimated for energy density of  $1.4 \text{ J/cm}^2$ .

The diffraction from 3D lattices which have the multiple standing wave anti-nodes along axial direction leads to the mutual interference of the beams diffracted from the transverse structures in each anti-node. The formation of anti-node planes parallel to the crystal surface with half-wavelength period in axial direction results also to the back diffracted beams at the Bragg angle. This, in turn, decreases the forward diffracted power for 3D lattice. This is in agreement with the results of measurements of diffraction efficiency for 2D and 3D lattices by registration of forward diffracted power stated in Sect. 6.

The energy invested into the photorefractive LN:Fe crystal due to the absorption during the formation of 3D lattice by CIM technique is larger compared with the case of recording of 2D lattice without back-reflecting mirror. The cause is the multiple traversing of the beam through the crystal in the scheme of formation of 3D grating with back-reflecting mirror due to reflections from the mirror with  $r = 95 \%$  and from front surface of crystal with reflection coefficient of  $16 \%$ . The rough estimation showed that the energy absorbed by 0.5-mm-thick crystal at 532 nm with  $\alpha = 3.74 \text{ cm}^{-1}$  during multiple propagation of beam through the crystal, until its intensity will decrease by one order, is 2 times larger compared with the absorbed energy during single traversing of the beam through the crystal. Hence, 3D lattice should have higher depth of modulation in comparison with 2D lattice (see Fig. 8a, b).

### 9.3 Analysis of diffraction patterns from twofold RS lattices

The terminology “thin” and “thick” holographic grating is widely used for description of two diffraction regimes when multiple diffracted waves are produced (Raman-Nath regime) or only one diffracted wave is formed (Bragg regime) at nearly Bragg incidence of testing beam. The parameter  $Q' = Q/\cos \theta = 2\pi\lambda L/d^2 n_0 \cos \theta$ , where  $L$  is grating thickness,  $\lambda$  is vacuum wavelength of the light,  $d$  is grating period,  $n_0$  is mean refractive index,  $\theta$  is angle of incidence of light to the grating [10], is often used to distinguish between thin ( $Q' < 1$ ) and thick ( $Q' > 10$ ) gratings. However, this parameter does not take into account the grating strength, i.e., refractive index modulation depth. Various authors have observed several diffracted waves from hologram even when  $Q$  was large (see [53] and references therein). The description of diffraction regimes with criteria which include the effect of grating strength is also suggested (see, for example [54]). The grating strength is given by  $\gamma = \pi \Delta n L/\lambda$ , where  $\Delta n$  is the refractive index change. Two criteria  $\gamma Q' < 1$  and  $Q'/2 \gamma > 10$  define the thin and thick gratings, respectively.

The thick holographic grating may be described also as a grating exhibiting strong angular selectivity [54]. Thick grating behavior may be considered to occur when parameter  $L/d > 10$ . The thin grating is characterized by  $L/d \leq 10$ . The diffraction efficiencies of the gratings depend also on the shape of grating and are different for sinusoidal and non-sinusoidal gratings, which is more pronounced for higher-order diffractions and is larger for non-sinusoidal gratings [55, 56].

Twofold RS masks used for lattices formation are an example of multi-periodical structures in the transverse plane. The 3D lattices recorded in photorefractive crystal by CIM method have micrometric scale multi-periodicity in the transverse plane and sub-micrometric scale half-wavelength periodicity in the axial direction. In the analysis of the diffraction patterns from such complex lattices, the formation of rectangular grating along  $C$ -axis and sinusoidal grating perpendicular to the  $C$ -axis of the crystal also should be taken into account. The sinusoidal grating produces only zeroth and  $\pm 1$  diffraction orders, while the rectangular grating considered as consisting of sinusoidal Fourier components forms multiple diffraction orders [10]. From this point of view, the diffraction from lattices recorded with orientation of  $C$ -axis of the crystal along vertical  $Y$  and horizontal  $X$  directions can give different results.

1. Orientation of  $C$ -axis of the crystal along vertical direction during recording.

The observed pronounced stretching of diffraction orders in vertical  $Y$  direction for 2D lattice (Fig. 5a) can be

understood taking into account different periodicity of twofold RS lattice along horizontal  $X$  and vertical  $Y$  directions. The recorded 2D lattices have smaller period in  $X$  directions ( $d_X \sim 20 \mu\text{m}$ ) compared with periods in  $Y$  direction ( $d_Y \sim 40\text{--}60 \mu\text{m}$ ) (Fig. 3a).

Based on the estimation of refractive index change  $\Delta n = 0.6 \times 10^{-4}$  for  $L = 0.5 \text{ mm}$ , the parameters  $Q'$  and  $\gamma$  are estimated of  $Q' = 2$  for  $d_X \sim 20 \mu\text{m}$  and  $\gamma \sim 10^{-1}$ . Thus,  $Q'/2 \gamma \sim 10$  which corresponds to the Bragg regime with first-order diffracted waves in the  $X$  direction.

Similar estimations for gratings period of  $d_Y \sim 40 \mu\text{m}$  give the values of  $Q' = 0.5$  and  $\gamma Q' \sim 5 \times 10^{-2}$ , which correspond to Raman-Nath regime with multiple diffraction orders in  $Y$  direction.

The angular selectivity parameter of recorded lattice along  $X$  direction with the value of  $L/d_X \approx 25$  is also larger compared with the value of  $L/d_Y \approx 8\text{--}12$  along  $Y$  direction. This leads to the same conclusion of the formation of first-order diffraction in the horizontal  $X$  direction and multiple diffraction orders in the vertical  $Y$  direction.

The formation of rectangular lattice along vertically oriented  $C$ -axis also assists the appearance of multiple diffraction orders in vertical  $Y$  direction, whereas the formation of sinusoidal grating perpendicular to  $C$ -axis provides only the first-order diffraction.

3D refractive lattices recorded by CIM technique are thick gratings since the criteria  $Q \sim 10^4 \gg 10$  and  $L/d_z \approx 1,879 \gg 10$  for  $L = 0.5 \text{ mm}$  and  $d_z = 266 \text{ nm}$  are satisfied along the axial direction. The 3D thick lattice reveals more angular selectivity and shows less diffraction orders (Fig. 5b) compared with 2D lattice (Fig. 5a). The appearance of weak second-order diffraction can be attributed to the rectangular shape of the grating and its higher modulation depth.

## 2. Orientation of $C$ -axis of the crystal along horizontal direction during recording.

The diffraction patterns obtained when recording of the lattice was performed with  $C$ -axis of the crystal oriented in horizontal  $X$  directions are shown in Fig. 5c, d. For 2D lattice, more powers are diffracted along horizontally oriented  $C$ -axis (Fig. 5c). The second-order diffraction lateral petals are clearly seen in Fig. 5c. For this configuration, the rectangular grating formed along  $C$ -axis assists the appearance of multiple diffraction orders, whereas the large parameters of  $Q'/2 \gamma \sim 10$  and  $L/d_X \approx 25$  limit the appearance of higher-order diffractions. The combined actions of two effects result in the appearance of only second-order diffraction along  $C$ -axis. The sinusoidal grating formed perpendicular to the  $C$ -axis provides the first-order diffraction in vertical  $Y$  direction (Fig. 5c). 3D lattice exhibiting stronger angular selectivity shows only the first-order diffraction (Fig. 5d).

Since 3D lattice has a half-wavelength period in the axial direction corresponding to the spatial frequency of  $K \sim 4 \times 10^4 \text{ lines/cm}$ , the diffusion of photo-charges which takes place along all directions also contributes to the grating formation, however, with less efficiency than photovoltaic effect. The contribution of photovoltaic effect and diffusion mechanisms in refractive lattices formation was studied in detail for 1D and 2D lattices formation by Bessel beam technique in [30, 50].

## 9.4 Prospects of formation of 3D periodic and quasi-periodic structures in photorefractive crystals and applications

The lifetime of recorded lattices in the doped lithium niobate crystals in the absence of external effects, such as light (dark storage time) and heating, is up to 1 year [7, 57, 58]. In particular, the detailed study of the recorded 1D grating in iron-doped lithium niobate crystals showed [57, 58] that the dark storage time varies from few minutes to 1 year depending on the concentration of the iron and crystal temperature. At room temperature, the dark storage time of the recorded lattices in LN:Fe and LN:Fe:Cu crystals used in the present experiment is around 1 year.

Apart the long period fixing of photonic lattices in photorefractive crystals, the recorded structures can be erased by homogeneous light, more effectively by intense UV light, thus allowing the multiple recording of photonic structures in the crystal.

The diffraction efficiency of the recorded lattices by CIM method can be increased by optimization of the parameters of experiment and used crystals and by increasing of the intensity of recording beam, which will make the proposed photonic lattices more suitable for applications.

Considering the intensity-modulated laser beam as an encoded information carrier, the recording of the photonic lattices in the crystal corresponds to recording and storage of information with the possibility of further readout. The readout results in the light diffraction and reconstructs the information encoded in the recording spatially modulated beam. From this point of view, the erasure of the stored lattices (i.e., stored information) during readout by homogeneous light is a preventing factor and limits the possibility of multiple readouts. One of the ways to avoid the erasure of stored lattice is the readout by longer wavelength laser beam than the recording wavelength, which prevents the excitation of photo-electrons from impurity ions to the conduction band [23]. This method was used in the present experiment. For many applications, more convenient is to perform the readout by uniform probe beam at the recording wavelength. Very promising is two-photon

recording [59] in materials in which two photons are required for generation of free electrons. The other method is two-center holographic recording in doubly doped photorefractive crystals, suggested and realized with the use of LN:Fe:Mn crystal and two-beam interference technique in [23]. The doubly doped LN crystals exhibiting photochromic effect, i.e., the increase in absorption coefficient with increase in light intensity [23, 60], provide the high stability of stored grating during readout by weaker probe beam at the recording wavelength. The detailed studies of two-center recording by Bessel standing wave technique [30] with 17 mW, 532 nm beam in LN crystal doped with 0.05 wt% of Fe and Cu showed the persistence of recorded gratings against erasure during 8,000 s when illuminating by 2 mW homogeneous probe green beam [60]. LN:Fe:Cu crystal also was used in our experiments for 2D and 3D lattices recording and showed more persistence against erasure compared with LN:Fe crystal. This feature was used for white light testing of dispersive properties of recorded refractive lattices.

The suggested combined interferometric–mask method is simpler compared with technique of multi-exposure of two-beam [37] and multi-beam interference patterns [38], realized for fabrication of 2D and 3D quasi-periodic structures in photosensitive materials. The use of different rotational symmetry masks will allow the formation of quasi-crystalline structures. The structuration along axial direction with sub-micrometric scale periodicity is achieved easy and is determined by the standing wave periodicity, which can be varied by the use of recording lights with different wavelength. The disadvantage of the method is that the masks printed on the transparent film lose the initial contrast after few tens 1 h exposition during recording under influence of 100 mW green laser radiation. However, the preparation of the masks is very cheap. For comparison, the programmable SLM technique [39, 40] providing both amplitude and phase modulation of beam intensity profile is stable and flexible and allows the creation of reconfigurable higher rotational symmetry micro- and nanometric scale quasi-crystalline photonic lattices. Such lattices provide the isotropic and complete photonic bandgaps even in the materials with low refractive index contrast [34–36].

The suggested interferometric–mask method is very promising for 3D structuration of highly nonlinear media for studying of light localization and spatial soliton formation. The 2D soliton formation in structured media has been realized experimentally in limited number of works, in particular, in rectangular lattice [24] and in periodic ring lattice [26] in strontium barium niobate crystal. The light guiding and trapping systems, in turn, are promising for all-optical devices, optical storage, future communication systems, optical computers, etc.

## 10 Conclusions

The novel combined interferometric–mask technique is suggested and realized for the formation of 3D long-lived, high-contrast, micrometric and nanometric scale quasi-crystalline lattice structures of different symmetries in photorefractive materials. The novelty of the method is based on the combination of mask and interferometric (standing wave) techniques, which provides the three-dimensionality of the formed lattices. 2D different rotational symmetry diffraction masks with the periods of 20–60 micrometers were prepared. The interferometric testing of prepared masks by Gaussian beam was performed showing their high quality. Both 2D and 3D refractive lattices were recorded by mask and interferometric–mask technique in LN:Fe and LN:Fe:Cu crystals by 532 nm laser beam with the use of twofold RS masks. The recorded 2D and 3D refractive lattices were tested by the far-field diffraction pattern imaging and direct observation by phase microscope. The formed 3D rotational symmetry refractive lattices have 20–60  $\mu\text{m}$  periods in the radial direction, 60  $\mu\text{m}$  period along the azimuthal angle and half-wavelength 266 nm period in the axial direction. The refractive and dispersive properties of recorded lattices were studied. Physical mechanisms and prospects of optical induction of 2D and 3D photonic lattices in photorefractive crystals are discussed.

2D and 3D periodic and quasi-periodic artificial structures in photorefractive materials are promising for many applications, including guiding and trapping systems, photonic bandgap materials, all-optical devices, high capacity information storage and processing, spatial soliton formation, telecommunication systems, optical computers, etc.

**Acknowledgments** This work was supported by International Science and Technology Center Grant, Project A-1517 and National Grant of State Committee of Science of Armenia, Project 1-6/HK. The authors are grateful to Marina Derdzian for technical assistance and Dr. E. Kokanyan for providing of the lithium niobate crystals in the framework of ISTC Project.

## References

1. E. Yablonovitch, *Phys. Rev. Lett.* **58**, 2059 (1987)
2. J. Joannopoulos, S. Johnson, R. Meade, J. Winn, *Photonic Crystals* (Princeton University Press, Princeton, 2008)
3. S. Arishmar Cerqueira Jr, *Rep. Prog. Phys.* **73**, 024401 (1–21) (2010)
4. T.F. Krauss, R.M. De La Rue, *Prog. Quantum Electron.* **23**, 51–96 (1999)
5. C. Denz, M. Schwab, C. Weillnau, *Transverse-Pattern Formation in Photorefractive Optics* (Springer, Berlin, 2003)
6. K. Buse, C. Denz, W. Krolikowski, *Appl. Phys. B*, special issue **95**(3), 389–390 (2009)
7. P. Günter, J.P. Huignard, *Photorefractive Materials and Their Applications III* (Springer Series in Optical Sciences: Vol. 115, New York 2007)

8. R.A. Rupp, *Appl. Phys. A* **55**, 2–20 (1992)
9. W-H Lee, *Prog. Opt.* **XVI**, 121 (1978)
10. R.J. Collier, ChB Buckhard, L.H. Lin, *Optical Holography* (Academic Press, New York, 1971)
11. S. Chandrasekhar, *Liquid Crystals* (Cambridge University Press, Cambridge, 1977)
12. U. Bortolozzo, S. Residori, A. Petrosyan, J.P. Huignard, *Opt. Commun.* **263**, 317 (2006)
13. F. Simoni, G. Chipparrone, C. Umeton, G. Arabia, G. Chidichimo, *Mol. Cryst. Liq. Cryst.* **179**, 269 (1990)
14. R.A.M. Hikmet, J. Lub, *Prog. Polym. Sci.* **21**, 1165 (1996)
15. T.V. Galstian, L. Zohrabyan, A.M. Albu, E. Rusen, B. Marculescu, D.S. Vasilescu, *J. Nonlinear Opt. Quantum Opt.* **32**, 1 (2004)
16. H. Ren, Y.H. Fan, S.-T. Wu, *Appl. Phys. Lett.* **82**, 3168 (2003)
17. P. Cheben, M.L. Calvo, *Appl. Phys. Lett.* **78**, 1490 (2001)
18. F. Del Monte, P. Cheben, O. Martinez-Matos, J.A. Rodrigo, M.L. Calvo, *Adv. Mater.* **18**, 2014 (2006)
19. O. Martinez-Matos, J.A. Rodrigo, M.L. Calvo, F. Del Monte, *Appl. Phys. Lett.* **91**, 1411151 (2007)
20. M.L. Calvo, P. Cheben, *J. Opt. A Pure Appl. Opt.* **11**, 1 (2009)
21. T. Ackemann, W. Lange, *Appl. Phys. B* **72**, 21 (2001)
22. N. Korneev, O. Benavides, *JOSA B* **25**, 1899 (2008)
23. A. Adibi, K. Buse, D. Psaltis, *JOSA B* **18**, 584 (2001)
24. J.W. Fleischer, M. Segev, N.K. Efremidis, D.N. Christodoulides, *Nature* **422**, 147 (2003)
25. Y.V. Kartashov, V. Vysloukh, L. Torner, *Phys. Rev. Lett.* **93**, 093904 (2004)
26. X. Wang, Zh Chen, P.G. Kevrekidis, *Phys. Rev. Lett.* **96**, 083904 (2006)
27. J. Yang, I. Makasyuk, P.G. Kevrekidis, H. Martin, B.A. Malomed, D.J. Frantzeskakis, *Zh Chen, Phys. Rev. Lett.* **94**, 113902 (2005)
28. B. Terhalle, A.S. Desyatnikov, C. Bersch, D. Träger, L. Tang, J. Imbrock, Y.S. Kivshar, C. Denz, *Appl. Phys. B* **86**(3), 559 (2007)
29. G. Zito, B. Piccirillo, E. Santamato, A. Marino, V. Tkachenko, G. Abbate, *Opt. Express* **16**(8), 5164 (2008)
30. A. Badalyan, R. Hovsepyan, P. Mantashyan, V. Mekhitarian, R. Drampyan, *J. Mod. Opt.* **60**, 617 (2013)
31. P. Rose, F. Diebel, M. Boguslawski, C. Denz, arXiv:1202.5724.v1 [Phys. Opt.] (2012)
32. P. Rose, M. Boguslawski, C. Denz, *New J. Phys.* **14**, 033018 (2012)
33. Z.M. Stadnik, *Physical Properties of Quasicrystals* (Springer, Berlin, 1999)
34. M.E. Zorob, M.D.B. Charlton, G.J. Parker, J.J. Baumberg, M.C. Netti, *Nature* **404**, 740 (2002)
35. X. Chang, Z.Q. Zhang, C.T. Chan, *Phys. Rev. B* **63**, 081105R (2001)
36. W. Man, M. Megens, P.G. Steinhardt, P.M. Chaikin, *Nature* **436**, 993 (2005)
37. N.D. Lai, W.P. Liang, J.H. Lin, C.C. Hsu, C.H. Lin, *Opt. Express* **13**, 9605 (2005)
38. N.D. Lai, J.H. Lin, Y.Y. Huang, Ch. Ch. Hsu, *Opt. Express* **22**, 10746 (2006)
39. J. Xavier, P. Rose, B. Terhalle, J. Joseph, C. Denz, *Opt. Lett.* **34**, 2625 (2009)
40. J. Xavier, M. Boguslawski, P. Rose, J. Joseph, C. Denz, *Adv. Mater.* **22**, 356 (2010)
41. A. Badalyan, R. Hovsepyan, V. Mekhitarian, P. Mantashyan, R. Drampyan: International conference on laser physics 2010, ed. by Aram V. Papoyan, Proceedings of SPIE, Vol. 7998 (SPIE Bellingham, WA, 2011) 7998OH-1-10 (2011)
42. M.V. Berry, S. Klein, *J. Mod. Opt.* **43**, 2139 (1996)
43. A. Badalyan, R. Hovsepyan, V. Mekhitarian, P. Mantashyan, R. Drampyan, *Mol. Cryst. Liq. Cryst.* **561**, 57 (2012)
44. B. Kemper, G. von Bally, *Appl. Opt.* **47**, A52 (2008)
45. P. Bon, G. Maucort, B. Wattelier, S. Monneret, *Opt. Express* **17**, 13080 (2009)
46. F. Devaux, J. Safioui, M. Chauvet, R. Passier, *Phys. Rev. A* **81**, 013825 (2010)
47. F.S. Chen, *J. Appl. Phys.* **40**, 3389 (1969)
48. A.M. Glass, D. von der Linde, T.J. Negran, *Appl. Phys. Lett.* **25**, 233 (1974)
49. T. Avanesyan, E.S. Vartanyan, R.S. Mikaelyan, R.K. Hovsepyan, A.R. Pogosyan, *Phys. Stat. Sol. (a)* **126**, 245 (1991)
50. A. Badalyan, R. Hovsepyan, V. Mekhitarian, P. Mantashyan, R. Drampyan, International conference Photonics and Micro- and Nano-structured materials 2011, ed by R. Kh. Drampyan, Proceedings of SPIE, Vol. 8414 (SPIE, Bellingham, WA, 2012), 8414 OU (2012)
51. L.F. Kanaev, V.K. Malinovsky, B.I. Sturman, *Opt. Commun.* **34**, 95–100 (1980)
52. H. Kogelnik, *Bell Syst. Tech. J.* **48**, 2909 (1969)
53. M.G. Moharam, L. Young, *Appl. Opt.* **17**, 1757 (1978)
54. T.K. Gaylord, M.G. Moharam, *Appl. Opt.* **20**, 3271 (1981)
55. S.F. Su, T.K. Gaylord, *JOSA* **65**, 59 (1975)
56. R. Magnuson, T.K. Gaylord, *JOSA* **68**, 809 (1978)
57. Y. Yang, I. Nee, K. Buse, D. Psaltis, *Appl. Phys. Lett.* **78**, 4076 (2001)
58. I. Nee, M. Muller, K. Buse, E. Kratzig, *J. Appl. Phys.* **88**, 4282 (2000)
59. D. Von der Linde, A.M. Glass, K.F. Rodgers, *Appl. Phys. Lett.* **25**, 155 (1974)
60. P. Mantashyan, International conference on laser physics 2010, ed. by A.V. Papoyan, Proceedings of SPIE Vol. 7998 (SPIE Bellingham, WA, 2011) 7998 OJ-1-8 (2011)